Anisotropic Particle Multiphase Equilibria in Nonuniform Fields

*Philippe B. Baron, Rachel S. Hendley & Michael A. Bevan**
Chemical & Biomolecular Engr., Johns Hopkins Univ., Baltimore, MD 21218, USA

Abstract

We report a method to predict equilibrium concentration profiles of hard ellipses in nonuniform fields including multiphase equilibria of fluid, nematic, and crystal phases. Our model is based on a balance of osmotic pressure and field mediated forces by employing the local density approximation. Implementation of this model requires development of accurate equations of state for each phase as a function of hard ellipse aspect ratio in the range k=1-9. Predicted density profiles display overall good agreement with Monte Carlo simulations for hard ellipse aspect ratios k=2,4,6 in gravitational and electric fields with fluid-nematic, fluid-crystal, and fluid-nematic-crystal multiphase equilibria. Profiles of local order parameters for positional and orientational order display good agreement with values expected for bulk homogeneous hard ellipses in the same density ranges. Small discrepancies between predictions and simulations are observed at crystal-nematic and crystal-fluid interfaces due to limitations of the local density approximation, finite system sizes, and uniform periodic boundary conditions. The ability of the model to capture multiphase equilibria of hard ellipses in nonuniform fields as a function of particle aspect ratio provides a basis to control anisotropic particle microstructure on interfacial energy landscapes in diverse materials and applications.

Introduction

The ability to manipulate anisotropic colloidal particle microstructures in external fields provides a basis to design, control, and optimize particle-based materials and devices. The ability to control two-dimensional microstructures of anisotropic particles on surfaces can be used to define a number of interfacial properties (e.g., optical, electromagnetic, adhesive, wetting, etc.) in synthetic[1] and natural materials.[2-3] Because kinetic factors often limit the degree of order obtained in the assembly of anisotropic particles on surfaces,[4-5] external fields are often employed to mediate interactions and influence kinetic pathways.[6-10] As such, understanding equilibrium phases of anisotropic particles in nonuniform fields on surfaces is essential to understand achievable target free energy minimum microstructures. Understanding how multiple phases (*e.g.*, liquid, liquid crystal, crystal) can occur in spatially varying nonuniform fields could enable patterning of hierarchical surface materials (*e.g.*, analogous to multifunctional insect exoskeleton surfaces[11]) and reconfigure microstructured surfaces in devices (*e.g.*, colloidal displays analogous to liquid crystal displays,[12] microchip assembly[13]).

The two-dimensional phase behavior of a number of particle shapes has been well-studied in bulk homogeneous systems in the absence of fields. In particular, disks, ellipses, squares, rectangles, and other rounded variants have been the subject of many modeling studies, which are all hard superellipse shapes.[14] Other than hard disks, perhaps the simplest of these shapes is the hard ellipse, for which phase behavior and equations of state have been characterized.[15-18] Bulk homogeneous phase behavior of hard ellipses as a function of concentration and aspect ratio includes isotropic fluid, nematic, plastic crystal, and crystal phases. Although spherical particles

* To whom correspondence should be addressed: mabevan@jhu.edu

have been studied in nonuniform two-dimensional electric fields,[19-20] we are unaware of any studies quantifying two-dimensional phase behavior of different particle shapes in such fields.

Multiphase equilibria of different particle shapes in external fields have primarily been investigated in three dimensional systems within gravitational fields (*i.e.*, sedimentation equilibrium). Sedimentation equilibrium studies of spherical colloids have been studied since the early pioneering work of Perrin,[21] and are now sufficiently well understood to routinely invert density profiles as a measure of colloidal phase behavior and equations of state.[22-23] Experimental sedimentation equilibrium studies of clay platelets,[24] silica rods,[25] and mineral rod-plate mixtures[26] have shown good agreement with bulk phase diagrams, which have been supported by careful modeling studies.[27-28] Practically, the majority of experimental studies to date have probed multiphase equilibria in uniform gravitational fields on macroscopic scales much greater than particle dimensions (with some exceptions[29-30]). Although it is well established that anisotropic colloidal particles (*e.g.*, minerals, viruses, etc.) form liquid crystals in uniform external electric and magnetic fields,[31] there has been little characterization of anisotropic particles within local nonuniform external fields.[32]

Here, we model the position dependent phase behavior of hard ellipses on spatially varying energy landscapes due to nonuniform fields (**Fig. 1**, *e.g.*, gravity, electric fields as in recent experiments[9-10]). We develop a general model to determine concentration profiles within coexisting liquid, liquid crystal, and crystal phases for nonuniform fields based on the balance of local osmotic pressure and field mediated particle compression. To implement this model for hard ellipses, we develop simple and accurate equations of state for hard ellipse fluid, nematic, and crystal phases as a function of aspect ratio, based on prior theories and simulation results. We compare model predictions with Monte Carlo (MC) simulations for a number of illustrative cases involving multiphase equilibria of fluid, nematic, and crystal states for different hard ellipse aspect ratios, field types/shapes, and particle orientations. We further characterize spatially varying microstructure within inhomogeneous phases using local order parameters to color renderings and produce order parameter profiles. By developing the ability to predict local phase behavior in spatially varying nonuniform fields, our findings provide a basis to design, control, and optimize field properties to achieve desirable spatially varying surface microstructures and associated emergent material properties.

Theory

System Overview

This work investigates hard ellipses in external fields (*e.g.*, gravitational, electric fields). The semi- major and minor axis lengths of each ellipse are a and b, and the aspect ratio is $k = a/b$. In lab coordinates, each ellipse has two translational degrees of freedom with position coordinates (x_i, y_i) and one rotational degree of freedom with angle coordinate (θ_i) as shown in (**Fig. 1**). In particle coordinates, the center-to-center distance between particle i and particle j is r_{ij}, and their relative angle is θ_{ij}. External fields in this work depend only on the lab x-coordinate.

In the following, predictions of hard ellipse concentration profiles in nonuniform fields are based on the Local Density Approximation (LDA),[33] where the local concentration corresponds to an equilibrium condition equivalent to a bulk system at the same concentration. The LDA is generally valid for concentration profiles where the dimensions of spatial gradients are large compared to particle dimensions. Despite this constraint, the LDA is often accurate on smaller scales than expected, as demonstrated in studies of sedimentation equilibria[27, 29, 34] and spherical

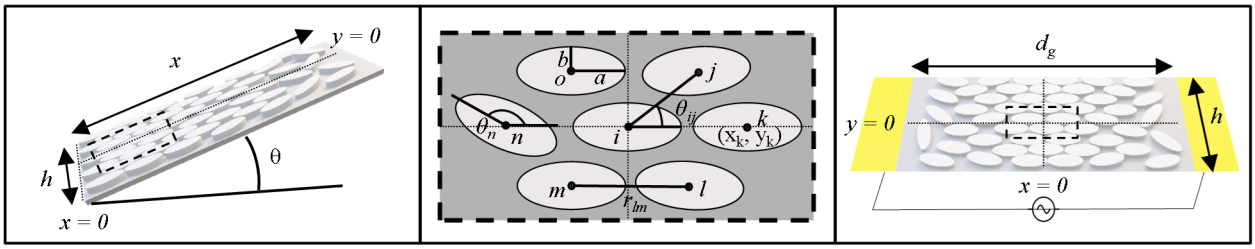

Fig. 1. Schematic of hard ellipses in gravitational and electric field mediated energy landscapes. (**left**) Laboratory coordinates for gravitational energy landscape on titled slide for sedimentation equilibrium. (**middle**) Particle dimensions and coordinates for both cases. (**right**) Laboratory coordinates for induced dipole in nonuniform electric field between parallel electrodes (yellow).

colloids on spatially varying landscapes.[20] Although a more general form, derived from Density Functional Theory, can be simplified using the LDA to arrive at the following expressions,[33-34] we start with a less general but simpler osmotic force balance based on the LDA. An alternative and equivalent impementation of the LDA based on local chemical potential may offer a convenient formulation for ease of implementation in uniform fields (*e.g.*, gravitational fields),[28] but such an approach has not been applied to multiphase equilibria in nonuniform fields.

Force Balance

We consider concentration profiles of hard ellipses in external fields where the profile and field depend only on the *x*-coordinate (**Fig. 1**). Under the conditions of the LDA, the equilibrium condition is given by a balance of the local osmotic pressure difference and the local force (*i.e.*, gradient of a scalar potential energy landscape) acting on the particles as,[19-20, 29, 35]

$$\Pi(x)-\Pi(x+\Delta x)=-\frac{du^{pf}(x)}{dx}\rho(x)\Delta x \tag{1}$$

where Π is osmotic pressure, $u^{pf}(x)$ is the particle-field potential (a one-dimensional, position-dependent energy landscape), and ρ is particle number density. For an infinitesimally small slice ($\Delta x \to 0$), Eq. (1) is,

$$\frac{d\Pi(x)}{dx}=-\frac{du^{pf}(x)}{dx}\rho(x) \tag{2}$$

and by inserting an appropriate equation of state to relate Π and ρ as,

$$\Pi(\rho)=k_BT\rho Z(\rho) \tag{3}$$

where k_B is Boltzmann's constant, T is absolute temperature, and Z is the compressibility factor, Eq. (2) becomes,

$$\frac{1}{\rho(x)}d\left(\rho(x)\cdot Z(\rho)\right)=-\frac{1}{k_BT}du^{pf}(x) \tag{4}$$

which can be integrated to give,

$$\int_{\rho_0}^{\rho(x)}\frac{1}{\rho}d\left(\rho\cdot Z\right)=-\frac{1}{k_BT}\left[u^{pf}(x)-u_0^{pf}\right] \tag{5}$$

where ρ_0 is a reference density, and u_0^{pf} is the potential energy at that density. Eq. (5) can be written in terms of area fraction, $\eta=\rho A_p$, where A_p represents the single particle area, as,

$$\int_{\eta_0}^{\eta(x)} \frac{1}{\eta} d(\eta \cdot Z) = -\frac{1}{k_B T}\left[u^{pf}(x) - u_0^{pf}\right] \tag{6}$$

which can be evaluated to determine $\eta(x)$ for a given $u^{pf}(x)$. Once $\eta(x)$ is obtained, the number of particles implied by the concentration profile by conservation of mass is given as,

$$N = \left(h / A_p\right) \int_{-0.5d_g}^{0.5d_g} \eta(x) dx \tag{7}$$

where h is the width (in the y-direction), and d_g is the range in the x-direction for the two-dimensional configuration in **Fig. 1**. Eq. (6) can be rearranged to obtain $Z(\eta)$ from $\eta(x)$ as,

$$\eta Z(\eta) - \eta_0 Z(\eta_0) = \int_{x_0}^{x} \frac{\eta(x)}{k_B T} \cdot \frac{du^{pf}(x)}{dx} dx \tag{8}$$

where x_0 is a reference location with an associated density η_0. In the present work we consider systems where density vanishes away from the origin, and taking $x_0 \to \infty$, we get $\eta_0 \to 0$ and $Z(\eta_0) \to 1$, which gives,

$$Z(\eta(x)) = \frac{-1}{\eta(x)} \int_{x}^{\infty} \frac{\eta(x)}{k_B T} \cdot \frac{du^{pf}(x)}{dx} dx \tag{9}$$

which provides a convenient method to approximate equations of state from particle distributions.

Hard Ellipse Phase Behavior & Equations of State

To calculate hard ellipse concentration profiles in fields, it is necessary to know hard ellipse phase behavior and equations of state. Hard ellipses exhibit different phases vs. aspect ratio, including: (a) isotropic, plastic crystal, and crystal phases for $1.0 < k \leq 1.6$, (b) isotropic and crystal phases for $1.6 \leq k \leq 2.4$, and (c) isotropic, nematic, and crystal phases for $k \geq 2.4$.[18] The isotropic-nematic transition (for $k \geq 2.4$) area fraction, η_N, vs. aspect ratio is given by,[17]

$$\eta_N = 6.37\left(5.14 + k\right)^{-1} \tag{10}$$

and for isotropic-solid coexistence ($1.6 \leq k \leq 2.4$) and nematic-solid coexistence ($2.4 \leq k \leq 9.0$), the highest area fraction fluid or nematic at freezing, η_F, and the solid area fraction at melting, η_M, vs. aspect ratio are well represented by,[18]

$$\eta_F = 0.5k^{-6.57} + 0.818 \tag{11}$$

$$\eta_M = 0.1k^{-3.5} + 0.833 \tag{12}$$

A number of studies have investigated equations of state for hard ellipse phases,[15-17, 36] but none of them capture simulation results for all aspect ratios, phases, and concentrations. These prior studies have suggested a form for the isotropic fluid compressibility factor, $Z_{I,HE}$, as,[16]

$$Z_{I,HE}\left(\eta, k\right) = 1 + \left[B_2(k)/2v_m\right]\left[Z_{F,HD}\left(\eta\right) - 1\right] \tag{13}$$

where $B_2(k)$ is the aspect ratio dependent second virial coefficient, v_m is particle volume, and $Z_{F,HD}$

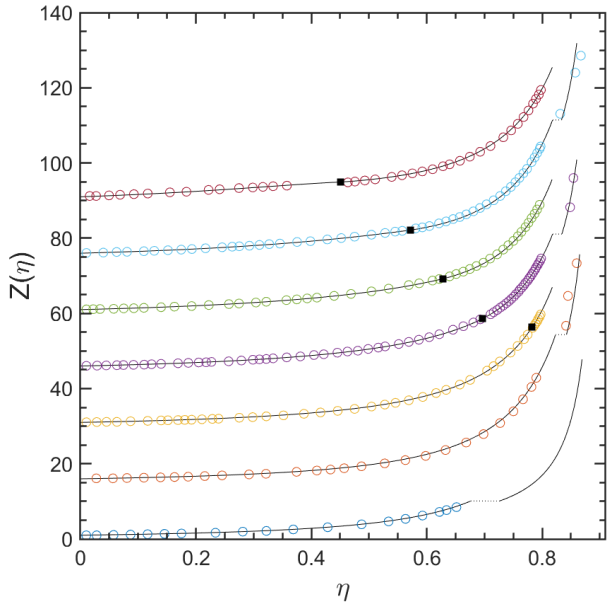

Fig. 2. Hard ellipse compressibility factor vs. aspect ratio for isotropic, nematic, and solid phases. Compressibility factor, Z, data for k = 1, 2, 3, 4, 5, 6, 9 (bottom-to-top) vs. area fraction, η. Z data for isotropic and nematic phases are from literature simulations.[17] Z data for solid phases are estimated from inversion of our MC simulated density profiles in **Figs. 3-5** using Eq. (9). Black squares indicate isotropic-nematic transition for $k > 2.4$ given by Eq. (10). Freezing and melting concentrations (bounding dashed coexistence line) for all aspect ratios given by Eqs. (11) and (12). Solid lines show equations of state for isotropic (Eq. (14)), nematic (Eq. (16)), and solid (Eq. (18)) phases.

is the hard disk fluid compressibility factor. [37] Based on this form, we developed an empirical correction to accurately capture reported compressibility factor data[17] (**Fig. 2**),

$$Z_{I,HE}(\eta,k) = 1 + \left[-0.12\eta^{2.5}(k-1)^2 + 0.21(k-1) + 1\right]\left[Z_{F,HD}(\eta) - 1\right] \tag{14}$$

which is applicable for aspect ratios $1.6 \le k \le 2.4$ for concentrations $0 \le \eta < \eta_F$, and for aspect ratios $2.4 \le k \le 9.0$ for concentrations $0 \le \eta < \eta_N$. This form is more accurate than the cited prior equations of state for ellipses that do not form a plastic phase ($1.6 \le k \le 9.0$), and it performs less well than recent scaled-particle theory results for slightly anisotropic ellipses ($1.0 \le k \le 1.6$).[17]

A density functional theory study of the hard ellipse nematic equation of state reports an additive correction to the hard ellipse isotropic fluid equation of state as,[15]

$$\begin{gathered} Z_{N,HE}(\eta,k) = Z_{I,HE}(\eta,k) - \eta I\left(Z_{F,HD}\right)\left[H(\gamma,\chi) - H_0(\chi)\right] \\ \chi = \left(k^2-1\right)/\left(k^2+1\right) \end{gathered} \tag{15}$$

where I is a function of the hard disk equation of state, H is the nematic phase excluded volume, γ is a critical nematic order parameter, and H_0 is the isotropic fluid excluded volume. Based on this form, we developed a semi-empirical nematic equation of state for hard ellipses to accurately capture reported compressibility factor data[17] (**Fig. 2**) as,

$$Z_{N,HE}(\eta,k) = Z_{I,HE}(\eta,k) + \left[2.27(\mathrm{k}-2.4)\left(\eta - \eta_N(k)\right)^{1.6}\right]\left[Z_{F,HD}(\eta) - 1\right] \tag{16}$$

which is valid for ellipses with aspect ratios $k \ge 2.4$ that exhibit a nematic phase for concentrations $\eta_N \le \eta < \eta_F$ (given by Eqs. (10) and (11)).

To estimate a solid crystal phase equation of state, we consider a form from free volume theory applied to anisotropic particles given as,[38-39]

$$Z_S(\eta) = 3\left[1-\left(\eta/\eta_{CP}\right)\right]^{-1} \tag{17}$$

where η_{cp} is the close packed solid volume fraction. We modify this form to maintain the functional divergence at close packing and include coefficients necessary for coexistence to give,

$$Z_{S,HE}\left(\eta,k\right) = Z_{X,HE}(k,\eta_F(k))\left[\frac{\eta_{cp}-\eta_M(k)}{\eta_{cp}-\eta}\right] \tag{18}$$

where X=I for aspect ratios $1.6 \le k \le 2.4$, and X=N for aspect ratios $2.4 \le k \le 9.0$. This form captures results from inverting (Eq. (9)) simulated density profile data (**Fig. 2**) as discussed in more detail in the following results and discussion section.

Interaction Potentials & Fields

For each particle in an nonuniform field, the potential energy is the sum of particle-field, u^{pf}_i, and particle-particle, u^{pp}_{ij}, potentials,[40]

$$u_i = u_i^{pf} + \sum_{j\neq i} u_{ij}^{pp} \tag{19}$$

where u^{pp}_{ij}, is a hard ellipse interaction (infinite for overlap and zero otherwise), and u^{pf} is a scalar field potential. In one case, we consider u^{pf} as a tangential component of gravity along a surface (*e.g.*, a tilted microscope slide surface, **Fig. 1**), which is linear in the coordinate, x, as,

$$u_g^{pf}(x) = Gz = Gx\sin\theta_T \tag{20}$$

where G is the buoyant colloid weight, and θ_T is a tilt angle. In a second case, we consider u^{pf} as a dipole-field interaction (induced dipole in non-uniform AC electric field, **Fig. 1**) as,[41-42]

$$u_i^{pf}(x) = -3V_p\varepsilon_m f_{cm}\left[E(x)\right]^2 \tag{21}$$

where x is particle position (**Fig. 1**), $E(x)$ is the position dependent electric field magnitude, ε_m is the medium dielectric constant, and f_{cm} is the Clausius-Mossotti factor.[43-45] The functional form for $E(x)$ was chosen based on exact models in our prior work,[44, 46-47] along with a modification based on an inverse analysis (using Eq. (6)) to modify the spatial distribution and boundaries of the inhomogeneous fluid, as given by,

$$E(x) = \left(\frac{V_{pp}}{8^{0.5}d_g}\right)\left(\frac{\left[2+1.268d^*\right]}{\pi\left[1.25+0.634d^*\right]}\right)\left[\frac{(0.27)^2}{d_g^2}\left(\frac{(0.27)^2}{d_g^2}+1\right)\right]^{-1/4}\left|\sin\left(\frac{\pi}{d_g}x\right)\right| \tag{22}$$

where V_{pp} is the peak-to-peak voltage of a sinusoidal AC electric field, and d_g is the electrode gap dimension (**Fig. 1**).

Order Parameters

To monitor local orientational order, we quantified each particle's nematic order as,[16, 48]

$$S_{2,i} = \max_{\theta_{2,i}}\left\langle\cos\left(2\left(\theta_j-\theta_{2,i}\right)\right)\right\rangle_{j\left(r_{ij}<6a\right)} \tag{23}$$

where r_{ij}, is center-to-center distance between particle i and neighboring particles j within six long axis radii, $6a$, and the local director direction, $\theta_{2,i}$, is calculated by maximizing the function. The value of $S_{2,i}$ varies from 0-1, where $S_{2,i}$ =1 indicates perfectly aligned orientation of all neighboring particles, and $S_{2,i}$ >0.5 is characteristic of local nematic structure. To monitor local positional order, we quantified each particle's stretched six-fold connectivity as,[49]

$$C_{6,i} = \frac{1}{6}\sum_{j=1}^{N_{b,i}}\left[\begin{vmatrix} 1 & \chi_6^{ij} \geq 0.32 \\ 0 & \chi_6^{ij} < 0.32 \end{vmatrix}\right], \quad \chi_6^{ij} = \frac{\left|\mathrm{Re}\left[\psi_{6,i}\psi_{6,j}^{*}\right]\right|}{\left|\psi_{6,i}\psi_{6,j}^{*}\right|} \tag{24}$$

where the local stretched bond orientational order parameter, $\psi_{6,i}$ (and its complex conjugate, $\psi^*_{6,i}$), are defined for anisotropic particles as,[14]

$$\psi_{6,j} = \frac{1}{N_{b,j}}\left|\sum_{k=1}^{N_{b,j}} \exp\left(i6\theta_{jk}\right)\right| = \frac{1}{N_{b,j}}\left|\sum_{k=1}^{N_{b,j}} \cos\left(6\theta_{jk}\right) + i\sin\left(6\theta_{jk}\right)\right| \tag{25}$$

where $N_{b,j}$ is the number of neighbors with bonds to particle j, and θ_{jk} is the angle of bonds between particle centers relative to an arbitrary axis. Neighboring particles are considered "bonded" if they are nearest neighbors in a Voronoi tessellation and fall within a threshold separation (halfway point between the first and second coordination shells in crystal state radial distribution function). The value of $C_{6,i}$ is normalized to vary from 0-1, where $C_{6,i}$=1 indicates 6 neighbors with perfect hexagonal bond orientational order.

Methods

Monte Carlo Simulations

Theoretical density profiles (Eqs. (6), (14), (16), (18), (20), (21)) were compared to canonical ensemble Monte Carlo (MC) simulations of hard ellipses. Particles were simulated in two dimensions (x, y) using the potentials in Eqs. (19)-(21), where the particle field potential depends on the x-coordinate, and the simulations have periodic boundary conditions in the y-coordinate. The particle, potential, field, and system parameters used in the MC simulations are reported in **Table 2**.

Table 2. MC simulation parameters for hard ellipses in AC electric fields based on prior experiments.[9, 44]

Parameter	Value	Parameter	Value
a, b, c (μm)	k, 1.0, 1.0	z (μm)	1.27
ρ_p (kg/m^3)	1960	$\varepsilon_p/\varepsilon_0$	3.8
ρ_m (kg/m^3)	1000	$\varepsilon_m/\varepsilon_0$	78
d_g (μm)	250-350	f_{cm} (k = 2)	-0.4190
f_{cm} (k = 4)	-0.4354	f_{cm} (k = 6)	-0.4422

Theoretical density profiles depend on three parameters: (1) the maximum packing fraction (η_{max}) at the particle-field potential energy minimum, (2) the total number of particles (N), and (3) the field magnitude determined for a gravitational field by θ_T in Eq. (20) and for electric fields by V_{pp} in Eq. (22). In particular, the density profile calculation in Eq. (6) requires defining η_{max} and V_{pp}, and then N is obtained from the mass balance equation in Eq. (7). Simulations were started from a stretched hexagonal lattice (η = 0.9069) in the system center. Equilibrium was achieved after ~500,000 steps. Simulated density profiles were averaged over 10 sets of ~10^3 independent configurations with each set sampled from an independent simulation.

To ensure no particle overlap, a three-step approximation was used as in previous studies.[14] The first approximation checks if the centers of the two particles being considered are more than twice the length of the particle semi-major axis away. If this condition is satisfied it ensures no overlap. If this condition fails, each ellipse is circumscribed in a rectangle and minimum distances between the particles are calculated. If these distances are positive, no overlap occurs, however, if they are nonpositive, a third approximation is used with checks points along a fine ellipse mesh. The ellipses are rotated and translated such that one ellipse is parallel to the laboratory x-axis and centered at the origin, then the following function is applied,

$$f(x,y)=\left[\frac{x}{a}\right]^2+\left[\frac{y}{b}\right]^2-1 \tag{26}$$

where (x, y) are points along the mesh of the non-centered ellipse. If this function returns any nonpositive value, then overlap occurs.

Results & Discussion

Hard Ellipse Sedimentation Equilibrium ($k=4$)

We first investigate the relatively simple case of hard ellipses (k=4) equilibrated in a gravitational field that is linear in the laboratory coordinate (e.g., along a microscope slide surface, Eq. (20)). This example is relevant to laboratory experiments with anisotropic colloidal particles and provides a straightforward comparison of the MC simulations and the model predictions (**Fig. 3**). We choose k=4 hard ellipses since they have isotropic, nematic, and crystalline phases for homogeneous infinite sized systems,[16-18] which provides a clear comparison for behavior of the same aspect ratio ellipses in inhomogeneous finite systems in the present work. The predicted density profile is given by the solid line in **Fig. 3** from Eq. (6) for the energy landscape in Eq. (20) using the equations of state for isotropic (Eq. (14)), nematic (Eq. (16)), and solid (Eq. (18)) phases. Transition concentrations are given by Eqs. (10)-(12), which correspond to bulk phase transition densities from published hard ellipse phase behavior.[17-18] We do not obtain estimates of phase boundaries directly from MC simulations (*e.g.*, by calculating free energies) but only compare MC simulated density profiles with predicted bulk homogeneous system transtion densities when constructing the density profiles. The particle number in the MC simulation was determined to be N=424 using Eq. (7), and the resulting simulated density profile is given by the points in **Fig. 3**.

The hard ellipse concentration profile predicted from Eq. (6) shows overall excellent agreement with the simulated concentration profile. The greatest systematic discrepancies are observed by a slight over prediction of the density at the isotropic-nematic transition and a slight under prediction of the density at the nematic-solid transition. These two systematic errors appear to preserve the area under the curve as required by the mass balance in Eq. (7). The density profile reaches the correct concentration in the solid phase at the potential energy minimum and vanishes as expected in the fluid phase. The overall good agreement demonstrates the accuracy of theory and its assumptions, as well as the suitability of the equations of state to capture the hard ellipse density in each phase including boundaries.

As a measure of spatially varying microstructure in MC simulated equilibrium configurations, we report position dependent local nematic order, S_2, and six-fold connectivity, C_6. These order parameter profiles capture local orientational and positional order of ellipses within inhomogeneous phases and across boundaries. In the crystalline phase, $C_6 \approx 1.0$ and $S_2 \approx 1.0$ exhibit

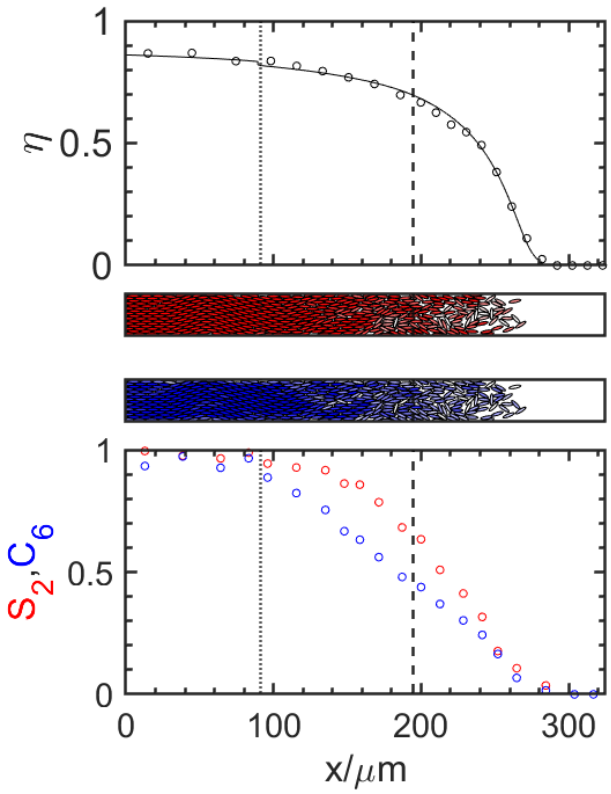

Fig. 3. Equilibrium concentration profile of k=4 hard ellipses in a gravitational field along a planar surface (e.g., colloids on tilted microscope slide). (**Top**) Predicted (Eq. (6), solid line) and MC simulated (points) (N=424 ellipses) density profile showing inhomogeneous solid phase transitioning to (vertical small dashed line, Eqs. (11),(12)) inhomogeneous nematic phase transitioning to (vertical large dashed line, Eq. (10)) inhomogeneous isotropic fluid with vanishing density at its periphery. (**middle**) MC simulation renderings colored by local S_2 (Eq. (23), red) and local C_6 (Eq. (24), blue). (**bottom**) Spatially varying order parameter profiles S_2(x) (red) and C_6(x) (blue) with phase transition locations indicated by same lines as top panel.

the expected high positional and orientational order, whereas both parameters drop rapidly in the fluid phase, particularly as density vanishes. Within the nematic phase, the nematic order is relatively high with $0.6 < S_2 < 1.0$ and six-fold connectivity is relatively lower with $0.5 < C_6 < 0.9$. Order parameter values at phase boundaries (vertical lines according to local density), including $S_2 \approx 0.6$ at the isotropic-nematic boundary and $C_6 \approx 0.9$ at the nematic-crystal boundary, are close to local and global values of these order parameters in homogeneous systems.[10, 14] Order parameter profiles display expected limiting and transition values corresponding to concentration dependent phase behavior, which provides additional validation of the observed behavior, and useful metrics for local microstructure.

Although local order parameter profiles in **Fig. 3** were implemented only to validate local phase behavior determined from density profiles, phenomenological or theoretical models relating local density and average local order parameters could enable predictions of order parameter profiles in nonuniform fields. Based on successful modeling of spatially varying hard ellipse phase behavior in a simple linear gravitational field, we next explore additional aspect ratios on more complex potential energy landscapes due to electric fields.

Low Aspect Ratio Hard Ellipses in Nonuniform Fields (k=2)

We next investigate phase behavior of low aspect ratio hard ellipses (k=2) on an energy landscape defined by a dipole-field potential (Eq. (21)) based on a nonuniform electric field between parallel electrodes (Eq. (22)). This energy landscape and field are typical of microscopy experiments involving induced dipolar interactions for anisotropic colloids in AC electric fields.[6-10] The potential energy minimum is at the electrode gap midpoint (**Fig. 1**, x=0), and the potential energy landscape is symmetric in the x-coordinate about the minimum. As a result, hard ellipses on this landscape have their highest concentration at the potential energy minimum, and the concentration decays symmetrically on either side of the minimum. The energy landscape in Eq. (21) depends on the electric field shape in Eq. (22), which can be adjusted by either changing the electrode gap dimensions, d_g, or the peak-to-peak voltage, V_{pp}.

We show concentration profiles for k=2 hard ellipses in a single electrode gap dimension with different numbers of particles and field amplitudes (**Fig. 4**). Hard ellipses of this aspect ratio do not form a stable nematic phase,[14-15, 18] so we explore this case first for a single phase inhomogeneous fluid and an inhomogeneous fluid coexisting with an inhomogeneous solid. The theory better captures the simulated non-uniform fluid phase alone but shows minor quantitative discrepancies near the fluid-solid transition in the case with coexisting phases. The order parameter profiles indicate minimal orientational or positional order everywhere in the inhomogeneous fluid case ($S_2 < 0.1$, $C_6 < 0.7$). In contrast, at the solid-fluid boundary in the case of coexisting phases, positional and orientational order in the simulation results persist at higher-than-expected values into the expected fluid region ($S_2 > 0.8$, $C_6 \approx 1$), which occurs spatially to about the same extent

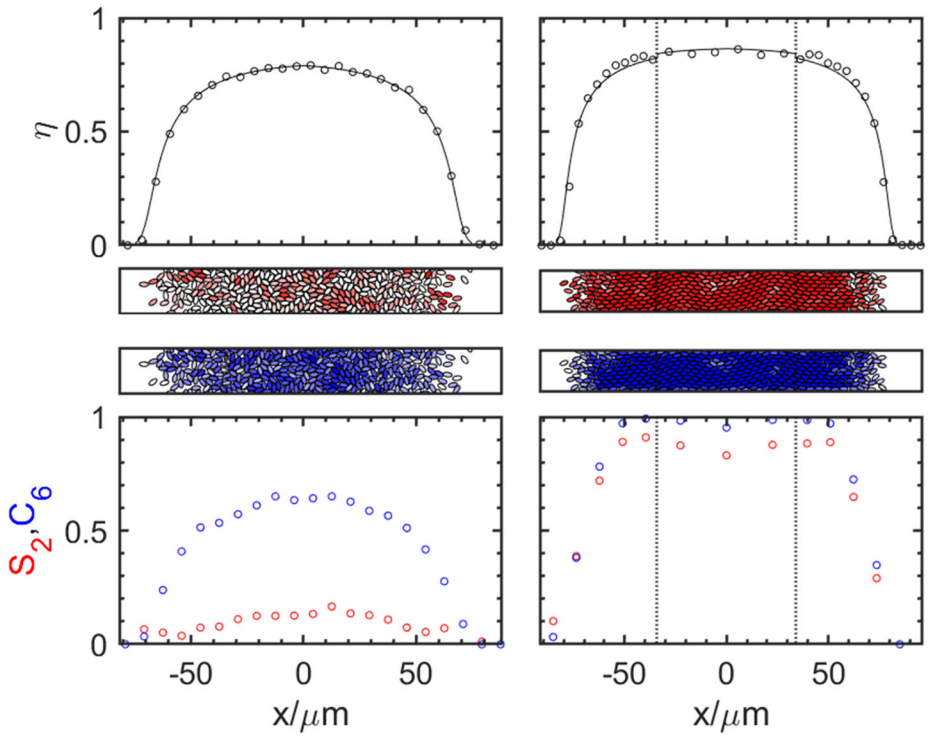

Fig. 4. Equilibrium concentration profiles for k=2 hard ellipses in a nonuniform electric field on a planar surface (e.g., colloids between parallel electrodes, Fig. 1). (**left**) N=357 hard ellipses with V_{pp} = 1.035 in Eq. (22), and (**right**) N=402 hard ellipses with V_{pp}=1.4500 in Eq. (22). Both systems were simulated with d_g = 250 μm in Eq. (22). (Top to bottom) Same information and formatting as **Fig. 3** panels.

where the simulated density is higher than the theoretical density.

To understand the discrepancy at the boundary for coexisting phases, we first note several features in the successful single phase inhomogeneous fluid case. In the single-phase, the maximum density of $\eta_{max} = 0.78$ at the potential energy minimum is just below the fluid-solid transition density for k=2 hard ellipses ($\eta_F \approx 0.81$, Eq. (11)). Despite the proximity to the transition density, the theory and simulation show exceptionally good agreement, and the simulated configurations show no evidence of local positional or orientational order associated with either a nematic or solid phase, even at the highest density.

In the fluid-solid coexistence case, the maximum density is $\eta_{max} = 0.864$ in the central region as expected for a solid phase. Near the fluid-solid interface, the simulated density is slightly lower than predicted on the solid side and slightly higher than predicted on the fluid side. The deviations on either side of the interface compensate each other as expected as part of satisfying the mass balance in Eq. (7). Because the fluid-solid interfacial width is finite, and the density changes on dimensions smaller than particle dimension, the LDA underlying the osmotic force balance in Eq. (6) is not obviously valid. Practically, the steep density gradient associated with positional and orientational correlations across the interfacial region is not expected to be well captured by the LDA, which likely accounts for all of the discrepancy in **Fig. 4**. However, despite this deficiency, the overall close proximity of the prediction in Eq. (6) to the simulated density profile is useful for nearly-quantitative predictions based on a relatively simple model (and compares well with similar approaches to sedimentation equilibrium of disks and anisotropic particles[27, 34]). We next explore how the LDA-based model performs for external field confinement of higher aspect ratio hard ellipses that form nematic phases and solid-nematic and nematic-fluid interfaces.

Moderate Aspect Ratio Hard Ellipses in Nonuniform Fields (*k=4*)

We next investigate k=4 hard ellipses in nonuniform electric fields. This particle geometry has sufficient anisotropy to form bulk homogeneous nematic phases. Results are reported at different field strengths and particle numbers for two-phase coexistence of fluid and nematic phases and three-phase coexistence of fluid, nematic, and crystal phases (**Fig. 5**). The left panels of **Fig. 5** show a nematic phase at the electrode center, with $\eta_{max} = 0.78$, coexisting with fluid phases on either side. The simulated and predicted (Eq. (6)) density profiles show excellent agreement at all positions including both phases and the interfacial region. In the nematic phase, $0.6<S_2<0.9$ and $0.5<C_6<0.6$ similar to the nematic phase values in the more gradual sedimentation equilibrium profile (**Fig. 3**), except the upper bounds are lower probably because the nematic phase does not share an interface with a solid phase in this case. The density and order parameters profiles and simulation renderings are all consistent with a central inhomogeneous nematic phase well described by the osmotic force balance (Eq. (6)) and nematic equation of state (Eq. (16)).

The right panels of **Fig. 5** show three-phase coexistence with a central $\eta_{max} = 0.86$ corresponding to a crystal phase. Overall, the simulated and predicted density profiles are in close correspondence at all positions within each phase. In the crystal region, $C_6 \approx 1$ and $S_2 \approx 1$, whereas in the nematic region, $0.7<S_2<1$ and $0.5<C_6<0.9$. The local order parameter profiles in the nematic phase on the left of **Fig. 5** more closely track the k=4 sedimentation equilibrium profile in **Fig. 3** that also has a crystal phase interface with the nematic phase, which appears to influence the upper limits in the nematic phase. On the nematic region periphery, the rapidly decaying density profile corresponds to an inhomogeneous fluid phase with low positional and orientational order.

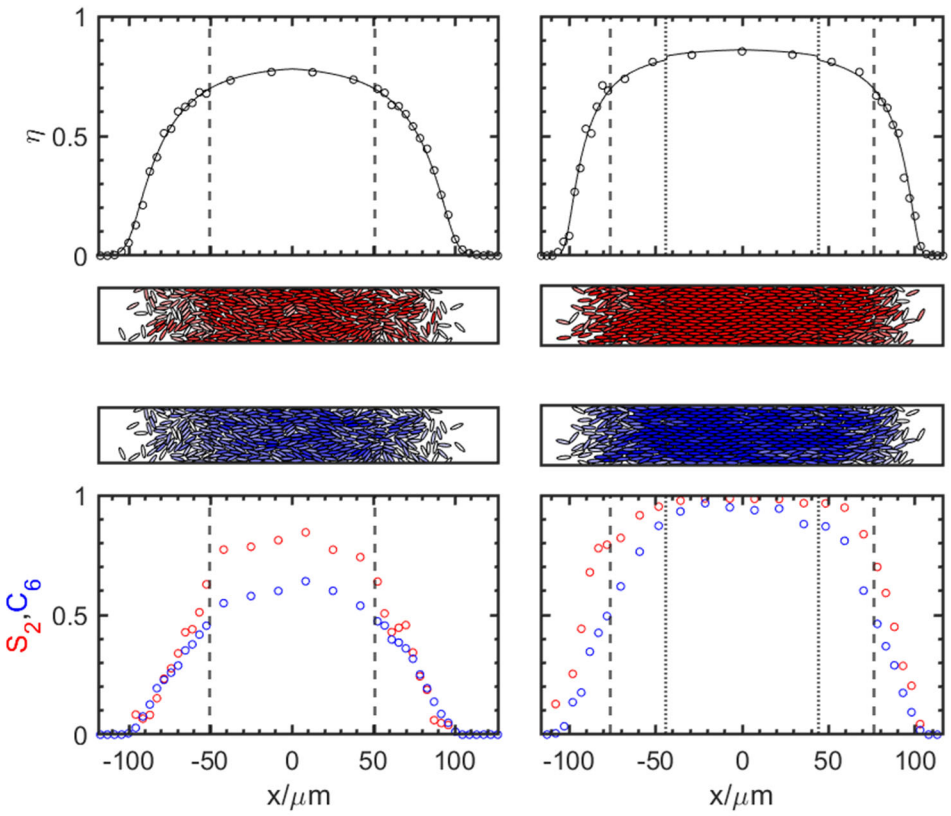

Fig. 5. Equilibrium concentration profiles for *k*=4 hard ellipses in a nonuniform electric field on a planar surface (e.g., colloids between parallel electrodes, Fig. 1). (**left**) N=340 hard ellipses with V_{pp} = 0.6845 in Eq. (22), and (**right**) N=410 hard ellipses with V_{pp}=0.967 in Eq. (22). Both systems were simulated with d_g =300 μm in Eq. (22). (Top to bottom) Same information and formatting as **Fig. 3** panels.

A notable aspect of the predicted density profiles in **Fig. 5** is the better quantitative and qualitative agreement with simulation results when the solid phase is not present, which is analogous to the k=2 hard ellipse results in **Fig. 4**. In both cases, the narrow crystal-nematic interface likely does not satisfy the conditions of the LDA as discussed in **Fig. 4**. This effect is seen in the slight underestimation of the density in the nematic phase near the nematic-crystal transition, as well as the gradual (rather than abrupt) order parameter changes across the crystal-nematic interface. Regardless, the prediction and simulation are in good agreement at nearly all concentrations, with only minor discrepancies at the crystal-nematic interfacial regions.

Close examination of the order parameter profiles and renderings in **Fig. 5** provides additional insights into the nature of the interfacial regions with some contrasts to the k=2 ellipses without a nematic phase. In particular, particles in the nematic region beyond the nematic-crystal interface (**Fig. 5**, right) should only have orientational order, but the C_6 order parameter profile indicates significant positional order. Because the nematic has high orientational order as well as high positional order, the effect of the finite width of the solid-nematic interface in the present case is a little harder to see than the width of the solid-fluid interface in the k=2 case (**Fig. 4**). Because the predicted density profile by itself appears quite accurate compared to the simulation, the additional local microstructural characterization is important to see the limit of the LDA in capturing interfacial microstructure in small inhomogeneous multi-phase systems with high density gradients on the order of particle dimensions.

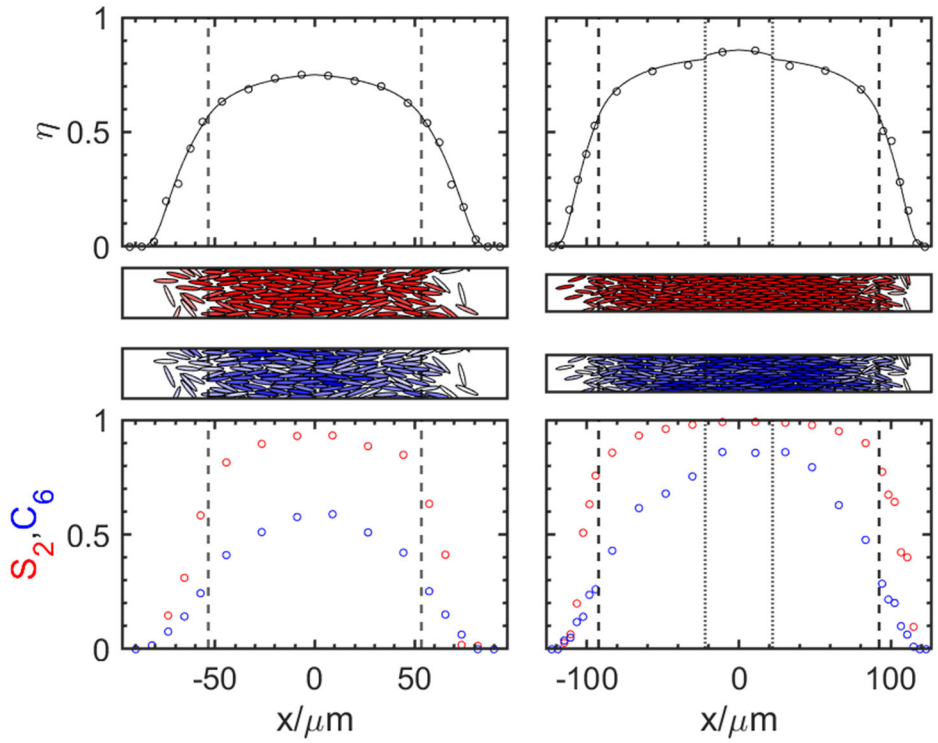

Fig. 6. Equilibrium concentration profiles for *k*=6 hard ellipses in a nonuniform electric field on a planar surface (e.g., colloids between parallel electrodes, Fig. 1). (**left**) N=306 hard ellipses with V_{pp} = 0.6845 in Eq. (22), and (**right**) N=377 hard ellipses with V_{pp}=0.7550 in Eq. (22). Both systems were simulated with d_g =350 μm in Eq. (22). (Top to bottom) Same information and formatting as **Fig. 3** panels.

High Aspect Ratio Hard Ellipses in Nonuniform Fields (k=6)

To further explore the predictive capability of Eq. (6),, we explore one additional higher aspect ratio (k=6) hard ellipse with the highest confinement relative the particle long axis dimension. Like k=4 ellipses, k=6 ellipses form up to three stable phases with two interfaces. **Fig. 6** shows results for (left) fluid-nematic coexistence and (right) fluid-nematic-crystal coexistence. Once again, the predicted and simulated density profiles show good agreement in both cases. The order parameter profiles show similar trends, features, and limiting values within each phase as in **Figs. 2-5**. The overall good agreement between the predicted and simulated density and microstructure profiles again shows the success of the simple osmotic force balance in small inhomogeneous multiphase systems of high aspect ratio hard ellipses.

One unique aspect of the k=6 hard ellipse results is the exceptionally small central crystal phase. The crystal phase is around 3-4 particle diameters across and is thus pushing the limits of the applicability of the LDA. This very small solid phase could explain the slightly lower values of C_6 observed for the crystal phase in this case compared to larger domains observed in all other cases tested thus far. Because C_6 is a measure of local crystallinity determined by ψ_6 values of nearest neighbors (Eqs. (24), (25)), the slightly lower values may just arise from the exceptionally small size of the crystal domain. However, somewhat related to this point, the crystal phase does not appear to persist into the nematic phase as much as other cases with crystal-nematic coexistence. Despite the slightly different quantitative and qualitative aspects of the crystal-nematic interface for the k=6 case, the small discrepancies can again be considered to result from

limitations of the LDA underlying Eq. (6).

Orientation Effects for Hard Ellipses in Nonuniform Fields (*k=4*)

Results in **Figs. 2-6** show the crystal-nematic interface is sensitive to spatial density changes across the interface relative to particle dimensions. In addition, the crystal interface appears to propagate positional order into the nematic phase through a sort of epitaxy, where particle long axes protruding from the crystal interface interdigitate with oriented particles in the nematic phase to produce extended positional correlations. Based on these observations, we investigate an additional case where the simulation is initialized with a central crystal region oriented with the particle minor axis parallel to the underlying energy landscape and direction of the density profile gradient. We use this different starting configuration to investigate two and three phase coexistence of k = 4 ellipses (**Fig. 7**). Practically, we aim to explore how orientation of the relatively shorter particle minor axis affects interfaces between phases. This case also provides a check on any orientation dependence of the osmotic force balance modeling approach.

The two-phase fluid-nematic case shows excellent agreement between predicted and simulated density profiles at all positions including the interfacial region (**Fig. 7**). Order parameter profiles also show typical values for each phase without any obvious issues at the nematic-fluid interface. The three-phase coexistence of fluid, nematic, and crystal phases in **Fig. 7**, also shows overall good agreement between predictions and simulations, although a discrepancy in density at the crystal-nematic interface shows greater disagreement than the same k=4 ellipses in the

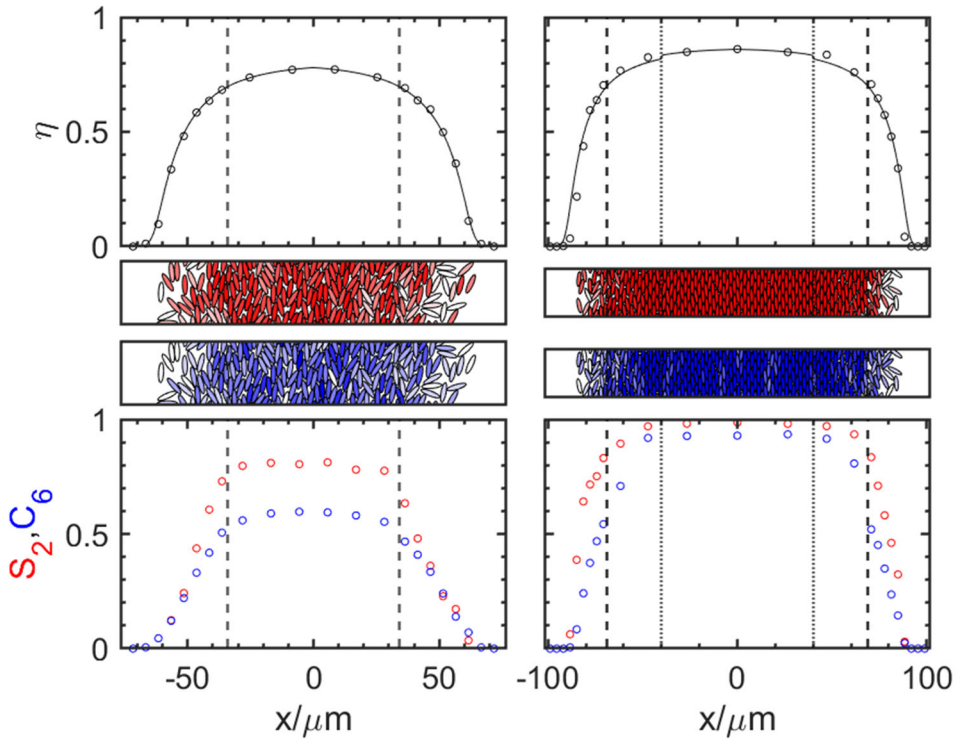

Fig. 7. Equilibrium concentration profiles for *k*=4 hard ellipses a nonuniform electric field on a planar surface (e.g., colloids between parallel electrodes, Fig. 1) (different alignment from Fig. 5). (**left**) N=357 hard ellipses with V_{pp} = 0.9170 in Eq. (22), and (**right**) N=425 hard ellipses with V_{pp}=1.033 in Eq. (22). Both systems were simulated with d_g =300 μm in Eq. (22). (Top to bottom) Same information and formatting as **Fig. 3** panels.

orthogonal orientation in **Fig. 5**. The order parameter profiles in this case are similar to the other case investigated with expected values in each phase except for higher-than-expected values in the nematic phase adjacent to the crystal-nematic interface.

The small disagreement in the predicted and simulated density profiles at the crystal-nematic interface is still likely a result of the validity of the LDA, but comparison of orientation effects with the same k=4 hard ellipses in **Fig. 5, 7** may suggest another contribution. Another potential issue to consider is finite system size effects in the y-direction (**Fig. 1**). Although the y-direction is orthogonal to the energy landscape and density variations in the x-direction, finite size effects could affect simulation results in a number of ways. Prior simulations of homogeneous anisotropic particles have shown greater nematic ordering for smaller system sizes (via the effective nematic phase elasticity).[50] Similar effects could influence nematic phases in either orientation in our simulated results as the result of finite size effects in the direction where the density is homogeneous. However, we note the inhomogeneous nematic phases in the absence of a crystal interface show good agreement between Eq. (6) and the simulations. Another potential issue is that the inhomogeneous crystal lattice cannot exactly match the periodic boundary in the y-direction for all densities in the x-direction. As such, the finite and incommensurate nature of the simulation box can be expected to also influence the crystal phase (as in our prior studies of sedimentation equilibria[29]). Taking these potential effects together, of the finite size and fixed periodic boundary condition, on both the nematic and crystal phases, it is possible these also contribute to the small discrepancies near the crystal-nematic boundary in all cases, in addition to limitations of the LDA. Ultimately, despite the small quantitative discrepancies between the model and simulations near the crystal-nematic interface, the model presented in this work provides overall excellent predictions of multi-phase coexistence of varying aspect ratio hard ellipses in highly non-uniform external fields.

Conclusions

We developed a model to predict density profiles of different aspect ratio hard ellipses in nonuniform external fields for coexisting fluid, nematic, and crystal phases. The model balances forces on particle due to external fields with the hard ellipse osmotic pressure based on the local density approximation (LDA). The model includes new simple accurate equations of state for hard ellipse fluid, nematic, and crystal phases as a function of aspect ratio (k =1-9), which fit our simulation results as well as established literature benchmarks. Predicted density profiles are in good agreement with MC simulation results for different aspect ratio particles in uniform gravitational fields and dipolar particles in nonuniform electric fields for cases with fluid-crystal, fluid-nematic, and fluid-nematic-crystal coexistence. Simulation renderings along with microstructural characterization via position dependent local order parameter profiles agree with expected values for homogeneous bulk phases. Minor discrepancies in density profiles are observed at phase boundaries with the greatest deviations at the crystal-nematic interfaces, where the LDA is expected to have the least validity based on the spatial density variations comparable to particle dimensions. Order parameter profiles show positional order propagates from the crystal-nematic interface into the region where a purely nematic phase is expected. Comparison of co-existing crystal and nematic phases with different orientations may also suggest finite size effects and uniform periodic boundary conditions could contribute the minor discrepancies between the model and simulation results. Our results show the overall success of the simple model for different hard ellipse aspect ratios, concentrations, multi-phase coexistence, and nonuniform fields, which demonstrates its utility for problems involving anisotropic colloidal-based materials and devices.

Acknowledgments

We acknowledge financial support by the National Science Foundation CBET 2113594.

References

1. Wu, N.; Lee, D.; Striolo, A. *Anisotropic Particle Assemblies*. Elsevier: Amsterdam, **2018**.
2. McDougal, A.; Miller, B.; Singh, M.; Kolle, M. Biological Growth and Synthetic Fabrication of Structurally Colored Materials. *Journal of Optics* **2019,** *21*, 073001.
3. Sanchez, C.; Arribart, H.; Giraud Guille, M. M. Biomimetism and Bioinspiration as Tools for the Design of Innovative Materials and Systems. *Nature Materials* **2005,** *4*, 277.
4. Liu, X.; Wang, H.; Zhang, Z.; Kosterlitz, J. M.; Ling, X. S. Nature of the Glass Transition in 2d Colloidal Suspensions of Short Rods. *New Journal of Physics* **2020,** *22*, 103066.
5. Zheng, Z.; Ni, R.; Wang, Y.; Han, Y. Translational and Rotational Critical-Like Behaviors in the Glass Transition of Colloidal Ellipsoid Monolayers. *Science Advances* **2021,** *7*, eabd1958.
6. Singh, J. P.; Lele, P. P.; Nettesheim, F.; Wagner, N. J.; Furst, E. M. One- and Two-Dimensional Assembly of Colloidal Ellipsoids in Ac Electric Fields. *Physical Review E* **2009,** *79*, 050401.
7. Famularo, N. R.; Hendley, R. S.; Boehm, S. J.; Guo, X.; Mayer, T. S.; Bevan, M. A.; Keating, C. D. Segmentation-Dependent Dielectrophoretic Assembly of Multisegment Metal/Dielectric Particles. *The Journal of Physical Chemistry C* **2020,** *124*, 18755-18769.
8. Kao, P.-K.; VanSaders, B. J.; Durkin, M. D.; Glotzer, S. C.; Solomon, M. J. Anisotropy Effects on the Kinetics of Colloidal Crystallization and Melting: Comparison of Spheres and Ellipsoids. *Soft Matter* **2019,** *15*, 7479-7489.
9. Hendley, R. S.; Torres-Díaz, I.; Bevan, M. A. Anisotropic Colloidal Interactions & Assembly in Ac Electric Fields. *Soft Matter* **2021,** *17*, 9066-9077.
10. Hendley, R. S.; Zhang, L.; Bevan, M. A. Design Rules for 2d Field Mediated Assembly of Different Shaped Colloids into Diverse Microstructures. *Soft Matter* **2022,** *18*, 9273-9282.
11. Sharma, V.; Crne, M.; Park, J. O.; Srinivasarao, M. Structural Origin of Circularly Polarized Iridescence in Jeweled Beetles. *Science* **2009,** *325*, 449-451.
12. Comiskey, B.; Albert, J. D.; Yoshizawa, H.; Jacobson, J. An Electrophoretic Ink for All-Printed Reflective Electronic Displays. *Nature* **1998,** *394*, 253-255.
13. Rupp, B. B.; Plochowietz, A.; Crawford, L. S.; Shreve, M.; Raychaudhuri, S.; Butylkov, S.; Wang, Y.; Mei, P.; Wang, Q.; Kalb, J.; Wang, Y.; Chow, E. M.; Lu, J. In *Chiplet Micro-Assembly Printer*, 2019 IEEE 69th Electronic Components and Technology Conference (ECTC), 28-31 May 2019; **2019**; pp 1312-1315.
14. Torres-Díaz, I.; Hendley, R. S.; Mishra, A.; Yeh, A. J.; Bevan, M. A. Hard Superellipse Phases: Particle Shape Anisotropy & Curvature. *Soft Matter* **2022,** *18*, 1319-1330.
15. Cuesta, J. A.; Tejero, C. F.; Baus, M. Isotropic-Nematic Transition of Hard Ellipses. *Physical Review A* **1989,** *39*, 6498-6506.
16. Cuesta, J. A.; Frenkel, D. Monte Carlo Simulation of Two-Dimensional Hard Ellipses. *Phys Rev A* **1990,** *42*, 2126-2136.
17. Xu, W.-S.; Li, Y.-W.; Sun, Z.-Y.; An, L.-J. Hard Ellipses: Equation of State, Structure, and Self-Diffusion. *The Journal of chemical physics* **2013,** *139*, 024501.
18. Bautista-Carbajal, G.; Odriozola, G. Phase Diagram of Two-Dimensional Hard Ellipses. *The Journal of Chemical Physics* **2014,** *140*, 204502.
19. Edwards, T. D.; Beltran-Villegas, D. J.; Bevan, M. A. Size Dependent Thermodynamics and Kinetics in Electric Field Mediated Colloidal Crystal Assembly. *Soft Matter* **2013,** *9*, 9208-

9218.
20. Zhang, J.; Zhang, Y.; Bevan, M. A. Spatially Varying Colloidal Phase Behavior on Multi-Dimensional Energy Landscapes. *J. Chem. Phys.* **2020,** *152*, 054905.
21. Perrin, J. *J. Phys. (Paris)* **1910,** *9*, 5.
22. Rutgers, M. A.; Dunsmuir, J. H.; Xue, J.-Z.; Russel, W. B.; Chaikin, P. M. Measurement of the Hard-Sphere Equation of State Using Screened Charged Polystyrene Colloids. *Phys. Rev. B* **1996,** *53*, 5043-5046.
23. Beltran-Villegas, D. J.; Schultz, B. A.; Nguyen, N. H. P.; Glotzer, S. C.; Larson, R. G. Phase Behavior of Janus Colloids Determined by Sedimentation Equilibrium. *Soft Matter* **2014,** *10*, 4593-4602.
24. Beek, D. v. d.; Schilling, T.; Lekkerkerker, H. N. W. Gravity-Induced Liquid Crystal Phase Transitions of Colloidal Platelets. *J. Chem. Phys.* **2004,** *121*, 5423-5426.
25. Kuijk, A.; Byelov, D. V.; Petukhov, A. V.; van Blaaderen, A.; Imhof, A. Phase Behavior of Colloidal Silica Rods. *Faraday Discussions* **2012,** *159*, 181-199.
26. van der Kooij, F. M.; Lekkerkerker, H. N. W. Liquid-Crystalline Phase Behavior of a Colloidal Rod-Plate Mixture. *Physical Review Letters* **2000,** *84*, 781-784.
27. Savenko, S. V.; Dijkstra, M. Sedimentation and Multiphase Equalibria in Suspensions of Colloidal Hard Rods. *Physical Review E* **2004,** *70*, 051401-1 - 051401-7.
28. Eckert, T.; Schmidt, M.; de las Heras, D. Gravity-Induced Phase Phenomena in Plate-Rod Colloidal Mixtures. *Communications Physics* **2021,** *4*, 202.
29. Beckham, R. E.; Bevan, M. A. Interfacial Colloidal Sedimentation Equilibrium I. Intensity Based Confocal Microscopy. *J. Chem. Phys.* **2007,** *127*, 164708.
30. Lu, M.; Bevan, M. A.; Ford, D. M. Closure-Based Density Functional Theory Applied to Interfacial Colloidal Fluids. *Langmuir* **2007,** *23*, 12481 -12488.
31. Lekkerkerker, H. N. W.; Vroege, G. J. Liquid Crystal Phase Transitions in Suspensions of Mineral Colloids: New Life from Old Roots. *Philosophical Transactions of the Royal Society A: Mathematical, Physical and Engineering Sciences* **2013,** *371*, 20120263.
32. Dozov, I.; Paineau, E.; Davidson, P.; Antonova, K.; Baravian, C.; Bihannic, I.; Michot, L. J. Electric-Field-Induced Perfect Anti-Nematic Order in Isotropic Aqueous Suspensions of a Natural Beidellite Clay. *J Phys Chem B* **2011,** *115*, 7751-65.
33. Hansen, J. P.; McDonald, I. R. *Theory of Simple Liquids*. Academic Press: London, **1986**.
34. Biben, T.; Hansen, J.-P.; Barrat, J.-L. Density Profiles of Concentrated Colloidal Suspensions in Sedimentation Equilibrium. *J. Chem. Phys.* **1993,** *98*, 7330-7344.
35. Juarez, J. J.; Feicht, S. E.; Bevan, M. A. Electric Field Mediated Assembly of Three Dimensional Equilibrium Colloidal Crystals. *Soft Matter* **2012,** *8*, 94-103.
36. Boublík, T. Equation of State of Hard Disk and 2d Convex Bodies. *Molecular Physics* **2011,** *109*, 1575-1580.
37. Henderson, D. Monte Carlo and Perturbation Theory Studies of the Equation of State of the Two-Dimensional Lennard-Jones Fluid. *Molecular Physics* **1977,** *34*, 301-315.
38. Stillinger, F. H.; Salsburg, Z. W. Limiting Polytope Geometry for Rigid Rods, Disks, and Spheres. *Journal of Statistical Physics* **1969,** *1*, 179-225.
39. Donev, A.; Burton, J.; Stillinger, F. H.; Torquato, S. Tetratic Order in the Phase Behavior of a Hard-Rectangle System. *Physical Review B* **2006,** *73*, 054109.
40. Tang, X.; Rupp, B.; Yang, Y.; Edwards, T. D.; Grover, M. A.; Bevan, M. A. Optimal Feedback Controlled Assembly of Perfect Crystals. *ACS Nano* **2016,** *10*, 6791-6798.
41. Jones, T. B.; Washizu, M. Equilibria and Dynamics of Dep-Levitated Particles: Multipolar

Theory. *J. Electrostatics* **1994,** *33*, 199-212.
42. Wang, X. B.; Huang, Y.; Burt, J. P. H.; Markx, G. H.; Pethig, R. Selective Dielectrophoretic Confinement of Bioparticles in Potential-Energy Wells. *J. Phys. D: Appl. Phys.* **1993,** *26*, 1278-1285.
43. Juarez, J. J.; Cui, J.-Q.; Liu, B. G.; Bevan, M. A. Kt-Scale Colloidal Interactions in High Frequency Inhomogeneous Ac Electric Fields. I. Single Particles. *Langmuir* **2011,** *27*, 9211-9218.
44. Rupp, B.; Torres-Diaz, I.; Hua, X.; Bevan, M. A. Measurement of Anisotropic Particle Interactions with Nonuniform Ac Electric Fields. *Langmuir* **2018,** *34*, 2497-2504.
45. Torres-Díaz, I.; Rupp, B.; Yang, Y.; Bevan, M. A. Energy Landscapes for Ellipsoids in Non-Uniform Ac Electric Fields. *Soft Matter* **2018,** *14*, 934-944.
46. Bahukudumbi, P.; Everett, W. N.; Beskok, A.; Huff, G. H.; Lagoudas, D.; Ounaies, Z.; Bevan, M. A. Colloidal Microstructures, Transport, and Impedance Properties within Interfacial Microelectrodes. *Appl. Phys. Lett.* **2007,** *90*, 224102.
47. Juarez, J. J.; Bevan, M. A. Interactions and Microstructures in Electric Field Mediated Colloidal Assembly. *J. Chem. Phys.* **2009,** *131*, 134704.
48. Narayan, V.; Menon, N.; Ramaswamy, S. Nonequilibrium Steady States in a Vibrated-Rod Monolayer: Tetratic, Nematic, and Smectic Correlations. *Journal of Statistical Mechanics: Theory and Experiment* **2006,** *2006*, P01005-P01005.
49. ten Wolde, P. R.; Ruiz-Montero, M. J.; Frenkel, D. Numerical Calculation of the Rate of Crystal Nucleation in a Lennard-Jones System at Moderate Undercooling. *J. Chem. Phys.* **1996,** *104*, 9932.
50. Frenkel, D.; Eppenga, R. Evidence for Algebraic Orientational Order in a Two-Dimensional Hard-Core Nematic. *Phys Rev A Gen Phys* **1985,** *31*, 1776-1787.